Combined local-density and dynamical mean field theory calculations for the compressed lanthanides Ce, Pr, and Nd

A. K. McMahan
Lawrence Livermore National Laboratory, University of California, Livermore, California 94550, USA
(Received 14 April 2005; revised manuscript received 21 July 2005; published 30 September 2005)

This paper reports calculations for compressed Ce ($4f^1$), Pr ($4f^2$), and Nd ($4f^3$) using a combination of the local-density approximation (LDA) and dynamical mean field theory (DMFT), or LDA+DMFT. The $4f$ moment, spectra, and the total energy among other properties are examined as functions of volume and atomic number for an assumed face-centered cubic (fcc) structure. These materials are seen to be strongly localized at ambient pressure and for compressions up through the experimentally observed fcc phases (γ phase for Ce), in the sense of having fully formed Hund's rules moments and little $4f$ spectral weight at the Fermi level. Subsequent compression for all three lanthanides brings about significant deviation of the moments from their Hund's rules values, a growing Kondo resonance at the Fermi level, an associated softening in the total energy, and quenching of the spin orbit since the Kondo resonance is of mixed spin-orbit character while the lower Hubbard band is predominantly $j=5/2$. While the most dramatic changes for Ce occur within the two-phase region of the γ-α volume-collapse transition, as found in earlier work, those for Pr and Nd occur within the volume range of the experimentally observed distorted fcc (dfcc) phase, which is, therefore, seen here as transitional and not part of the localized trivalent lanthanide sequence. The experimentally observed collapse to the α-U structure in Pr occurs only on further compression, and no such collapse is found in Nd. These lanthanides start closer to the localized limit for increasing the atomic number, and so the theoretical signatures noted above are also offset to smaller volume as well, which is possibly related to the measured systematics of the size of the volume collapse being 15%, 9%, and none for Ce, Pr, and Nd, respectively.

DOI: 10.1103/PhysRevB.72.115125 PACS number(s): 71.27.+a, 71.20.Eh, 75.20.Hr

I. INTRODUCTION

A number of the trivalent lanthanides undergo first-order phase transitions under pressure that are characterized by unusually large volume changes, Ce (15%),[1–3] Pr (9%),[4–8] Gd (5%),[9] and Dy (6%).[10] These "volume-collapse" transitions are believed to be caused by changes in the degree of $4f$ electron correlation from strongly correlated (localized) at pressures below the transitions to more weakly correlated (itinerant) at pressures above.[11–13] Associated with these two regimes are differences in physical properties, with high-symmetry crystal structures below the collapse transitions characteristic of metals without f electrons, and low-symmetry early-actinide-like structures at pressures above, suggesting a greater participation of f electrons in the bonding. The magnetic susceptibility is of Curie-Weiss character in the localized regime characteristic of Hund's rules $4f$ moments and is believed to become temperature independent similar to Pauli paramagnetism in the itinerant regime. The latter behavior has actually been observed only for the collapsed α phase of Ce, but is inferred for the other lanthanides based on analogies to the actinides.

In contrast to these apparently general trends, it has been recently shown that Nd reaches the characteristic itinerant α-U structure in a relatively continuous fashion without any phase transitions of unusually large volume change,[14] while in an analogous actinide system, Am is noted to undergo two collapse transitions.[15] Therefore, it would appear that the evolution from localized to itinerant character in these f electron metals occurs more generally in a continuous manner which may or may not be accelerated by one or more large-volume-change collapse transitions.

It was demonstrated many years ago that the volume-collapse transitions in the lanthanides and actinides do not involve the promotion of electrons from f to other states, and it was argued that these metals were instead undergoing Mott transitions in their respective $4f$ and $5f$ electron systems.[16,17] Local-density approximate (LDA) calculations modified to enable orbital polarization,[18–20] to include the self-interaction correction,[20–22] and to explicitly incorporate the Hubbard repulsion U_f[23,24] appear to provide such transitions for Ce and Pr. They describe large-volume magnetically ordered solutions with Hubbard split $4f$ bands, which become unstable under compression to paramagnetic solutions where these bands are grouped near the Fermi level. It has been suggested, however, that the rather abrupt delocalization of these modified-LDA transitions is an artifact of the static-mean-field nature of these techniques and that a correlated solution would allow a continuous transfer of f spectral weight between the Hubbard side bands and the Fermi level over an extended volume range.[25] This is the case for the Kondo-volume collapse model of the Ce transition, based on a many-body solution of the Anderson impurity model, which identifies Kondo-like screening of the local moment as the driving force for the transition.[26–28] More realistic calculations which combine LDA with correlated dynamical mean-field theory (DMFT),[29,30] so called LDA+DMFT,[31–33] generally corroborate these characteristics for Ce,[34–37] and the same technique has been applied to the actinides.[38]

Beyond the specific case of Ce, a more general understanding of the lanthanide volume-collapse transitions or their absence may come from putting them in context of the extended evolution from localized to itinerant character

which occurs as these materials are compressed. As a step in this direction, the present paper reports LDA+DMFT calculations over a wide range of volume for Ce ($4f^1$), Pr ($4f^2$), and Nd ($4f^3$), the last as mentioned being notable for the absence of a volume-collapse transition. These calculations have been carried out as in earlier work on Ce,[35,36] except that the spin-orbit interaction is now incorporated. They also assume a face-centered cubic (fcc) structure throughout, although LDA estimates of the structural energy differences suggest these are significantly smaller than the relevant contributions to the correlation energy, which may then be discussed in terms of their volume dependence as more important leading order effects.

The trivalent lanthanides follow a general structural sequence under pressure, namely hcp $\rightarrow$ Sm-type $\rightarrow$ dhcp $\rightarrow$ fcc $\rightarrow$ dfcc, where these abbreviations are for hexagonal close-packed (hcp), double hcp (dhcp), and distorted fcc (dfcc).[11–13] These are all just different stacking variants within the family of close-packed structures, except for dfcc, a soft L-point phonon distortion of fcc,[39] a phase which only Ce does not assume. The heaviest lanthanides traverse the full sequence, whereas the lighter ones begin part way, e.g., Ce, Pr, and Nd are all dhcp at ambient conditions, although fcc Ce is also metastable there. Since the same sequence is seen in Y, which has no nearby f states[40] and is theoretically understood to depend on the $5d$ occupancy,[41] it would appear to have no relation whatsoever with the f electrons, which are then presumed to be fully localized. Indeed, in the present work, we find evidence for fully formed Hund's rules moments and little $4f$ spectral weight at the Fermi level throughout the experimentally observed stability field of the fcc phases (γ for Ce) and for lower pressures.

Further compression takes Ce through a 15% volume collapse from the γ (fcc) to the α (also fcc) phase, while Pr undergoes a 9% collapse from the dfcc to an α-U structure, and Nd passes from the dfcc through two other low-symmetry structures before also reaching α-U, however, without any large volume changes. The present work finds a variety of signatures to accompany this compression regime: substantial deviation of the moments away from their Hund's rules values, rapid growth in $4f$ spectral weight at the Fermi level (the Kondo resonance) at the expense of the Hubbard side bands, an associated softness in the total energy, and quenching of the spin orbit due to the mixed-j character of the Kondo resonance versus the predominant $j=5/2$ lower Hubbard band. The most dramatic changes in these signatures for the case of Ce *coincide* with the two-phase region in the γ-α transition. This behavior was observed in earlier work on Ce[34–36] and is consistent with the Kondo-volume-collapse scenario.[26–28]

In regard to signatures in the total energy, a unique feature of the Kondo-volume-collapse model is the assertion that the γ-α transition is driven by a rapid drop in entropy from the γ to the α side, reflecting screening of the $4f$ moments. The transition, therefore, need not occur at $T=0$,[26,28] as has been documented for Ce alloys,[42] implying a featureless $T=0$ total energy. Nevertheless, due to the interrelationships between the different thermodynamic functions, and even though it is the free energy which actually determines the phase transition, the *finite-T* total energy should show an associated softening in the vicinity of the phase transition and is, therefore, a useful diagnostic.[43]

The present work finds the same signatures for compressed Pr and Nd; however, their most dramatic change takes place over the volume range where the dfcc phase is experimentally observed, suggesting this phase is of transitional character and not the end member of the localized trivalent lanthanide sequence as has been assumed. Only on further compression is Pr observed to collapse into the α-U structure, and as noted, Nd has no collapse. An important difference among the lanthanides is that they become more localized with increasing atomic number, due to the increased but incompletely screened nuclear charge. This is evident in the present work by the offset of the concurrent correlation-related signatures to smaller volumes from Ce to Pr and then to Nd. One consequence is that the softening effect in the energy associated with the growing Kondo resonance must compete with the remaining, dominant part of the energy which has a curvature that grows ever larger with decreasing volume. While a region of negative bulk modulus is required for an isostructural transition as in Ce, it may be more generally that a low bulk modulus favors larger volume changes in structural phase transitions, which would then be consistent with the decreasing size of the collapse from 15% (Ce) to 9% (Pr) to none (Nd). The observed collapse transitions in Gd and Dy would then appear inconsistent; however, these involve filling of the $j=7/2$ subshell, which complicates matters.

In the remainder of this paper, the theoretical methods are reviewed in Sec. II; numerical results for compressed Ce, Pr, and Nd are presented in Sec. III; and then a summary and discussion is given in Sec. IV.

II. THEORETICAL METHODS

The results in this paper, unless otherwise indicated, have been obtained by the LDA+DMFT(QMC) method, which refers to the merger of the local-density approximation (LDA) with dynamical mean-field theory (DMFT),[29,30] in order to create a composite technique[31–33] which rigorously treats on-site electron correlations and yet retains the material realism and specificity of the LDA. An essential component of the DMFT method is the solution of an auxiliary impurity problem, which is achieved here by a quantum Monte Carlo (QMC) algorithm.[44,45] The present calculations have been carried out as described in previous work for Ce,[35,36] except that the spin-orbit interaction has now been added and a broader set of materials considered. In the remainder of this section, we give a brief review of the method, various computational details, and the calculation of the moment.

A. The LDA+DMFT method

The LDA contribution to the LDA+DMFT method is to provide an effective Hamitonian which includes all valence electron degrees of freedom,

$$H = \sum_{\mathbf{k},ljm,l'j'm'} [H^0_{\mathrm{LDA}}(\mathbf{k})]_{ljm,l'j'm'} \hat{c}^\dagger_{\mathbf{k}ljm} \hat{c}_{\mathbf{k}l'j'm'} + \frac{1}{2} U_f \sum'_{\mathbf{i},jm,j'm'} \hat{n}_{\mathbf{i}fjm} \hat{n}_{\mathbf{i}fj'm'}. \quad (1)$$

Here, $\mathbf{k}$ are Brillouin-zone vectors; $\mathbf{i}$ are lattice sites; l is the orbital angular momentum; j is the total angular momentum ($l \pm \frac{1}{2}$ except just $\frac{1}{2}$ for $l=0$); $m=-j,-j+1,\ldots,j$; $\hat{n}_{\mathbf{i}fjm} \equiv \hat{c}^\dagger_{\mathbf{i}fjm} \hat{c}_{\mathbf{i}fjm}$; and the prime signifies $jm \neq j'm'$. The relevant valence states for the present lanthanide case are $6s$, $6p$, $5d$, and $4f$, and so the matrices $H^0_{\mathrm{LDA}}(\mathbf{k})$ are 32×32.

As described elsewhere,[13] the $H^0_{\mathrm{LDA}}(\mathbf{k})$ are orthogonalized one-electron Hamiltonian matrices obtained from converged linear muffin-tin orbital LDA calculations,[46–48] in which the $4f$ site energies are shifted so as to avoid double counting the f-f Coulomb interaction U_f, which is explicitly incorporated into Eq. (1). The spin-orbit interaction was included as a perturbation,[46] with the spin-orbit coupling parameters ξ_l kept fixed across the bands, although evaluated at the most important energies, namely at the respective centers of gravity of the occupied state density for each orbital type. The resultant $H^0_{\mathrm{LDA}}(\mathbf{k})$ matrices were calculated over a grid of volumes for Ce, Pr, and Nd in an assumed face-centered cubic (fcc) structure, and companion LDA constrained-occupation calculations were used to get the volume-dependent and material-dependent Coulomb interactions U_f.[13]

Dynamical mean-field theory assumes a local or $\mathbf{k}$-independent self-energy $\Sigma(i\omega)$, which together with the one-body part of Eq. (1) provides the lattice Green's function,

$$G_{\mathbf{k}}(i\omega) = [i\omega + \mu - H^0_{\mathrm{LDA}}(\mathbf{k}) - \Sigma(i\omega)]^{-1}. \quad (2)$$

This is solved in tandem with an auxiliary impurity problem defined by a similar Dyson-like equation with the same local self-energy.

$$G^{\mathrm{imp}}(i\omega) = [\mathcal{G}(i\omega)^{-1} - \Sigma(i\omega)]^{-1}. \quad (3)$$

The idea is to guess an initial $\Sigma = \Sigma^{(1)}$, calculate the lattice Green's function $G_{\mathbf{k}}$ from Eq. (2), identify its $\mathbf{k}$ average with G^{imp}, and then find the noninteracting or bath Green's function $\mathcal{G} = \mathcal{G}^{(1)}$ for the impurity problem from Eq. (3). The impurity problem is completely defined by $\mathcal{G}$, which describes its one-body part, together with the Coulomb interaction for its single site as in Eq. (1) without the $\mathbf{i}$ index. It may be solved exactly to within statistical uncertainties by QMC techniques.[44] This gives a new G^{imp}, which together with the input $\mathcal{G}^{(1)}$ defines a new self-energy $\Sigma = \Sigma^{(2)}$ again via Eq. (3). The cycle is then repeated by starting anew with $\Sigma = \Sigma^{(2)}$ in the lattice Green's function Eq. (2), and so on until self-consistency.

Quantities of interest such as the number n_j of $j=5/2$ or $7/2$ $4f$ electrons may be obtained from the lattice Green's function

$$n_j = \frac{T}{N} \sum_{n\mathbf{k}} \mathrm{Tr}_{fj}[G_{\mathbf{k}}(i\omega_n)] e^{i\omega_n 0^+}, \quad (4)$$

where the sums are over the $\mathbf{k}$ vector and Matsubara frequency $\omega_n = (2n+1)\pi T$, and the trace is over those $2j+1$ $4f$ states of type j. The total number of $4f$ electrons is then $n_f = n_{5/2} + n_{7/2}$. Similarly the energy per site for the effective Hamiltonian in Eq. (1) is

$$E_{\mathrm{DMFT}} = \frac{T}{N} \sum_{n\mathbf{k}} \mathrm{Tr}[H^0_{\mathrm{LDA}}(\mathbf{k}) G_{\mathbf{k}}(i\omega_n)] e^{i\omega_n 0^+} + U_f d, \quad (5)$$

which involves the double occupation,

$$d = \frac{1}{2} \sum'_{jm,j'm'} \langle \hat{n}_{fjm} \hat{n}_{fj'm'} \rangle, \quad (6)$$

as discussed elsewhere.[35,36] In principle, this is an average over the sites $\mathbf{i}$, although in practice we obtain this quantity from the QMC impurity problem.

To evaluate the total LDA+DMFT energy E_{tot} including all core and outer electrons, we add a correction to the paramagnetic all-electron LDA energy E_{LDA},

$$E_{\mathrm{tot}} = E_{\mathrm{LDA}} + E_{\mathrm{DMFT}} - E_{\mathrm{mLDA}}, \quad (7)$$

which consists of the DMFT energy E_{DMFT} from Eq. (5) less a LDA-like solution of the model Hamiltonian Eq. (1), thus "model LDA" or E_{mLDA}. To be more accurate, our LDA total energy E_{LDA} is scalar relativistic and so omits spin orbit; therefore, the correction E_{mLDA} should be and is obtained from a modification of Eq. (1) with the spin orbit removed. Using this modified effective Hamiltonian, E_{mLDA} is determined by a self-consistent solution of Eqs. (2) and (4) for $n_f = n_{5/2} + n_{7/2}$ taking a self-energy $\Sigma_{\mathrm{mLDA}} = U_f(n_f - \frac{1}{2})$. From this, the kinetic energy is calculated by the first term of Eq. (5) and the potential energy by $\frac{1}{2} U_f n_f (n_f - 1)$.

The simple form of Eq. (7) is a reminder of the still evolving nature of the LDA+DMFT method. There are recent discussions of the formal context of the method,[49] as well as some sense that a GW platform in place of the LDA may allow for more natural integration with DMFT.[50,51] Mutual self-consistency between the LDA and DMFT parts has also been stressed, i.e., feeding a different DMFT value of n_f back into a new LDA calculation.[38,49] This is impractical in the present case given the expense of the QMC solutions, although we do provide a perturbative change in n_f in going from the LDA to the DMFT, and this may well be sufficient. A step toward answering many of these questions is simply to provide more quantitative tests against the experiment of LDA+DMFT implementations with clearly stated approximations, and this is the spirit of the present work.

B. Computational details

While the matrices $G_{\mathbf{k}}$, $H^0_{\mathrm{LDA}}(\mathbf{k})$, and Σ in Eq. (2) are all 32×32, it is customary to take Σ nonzero only within the interacting or 14×14 f-f block, which permits the same reduction in the impurity problem itself. Even so, one must still determine seven distinct functions of ω to fill out $\Sigma(i\omega)$

even for the full cubic point group[52] and more otherwise. On the other hand, if we ignore the crystal field, then the f-f self-energy becomes

$$\Sigma_{jm,j'm'}(i\omega) = \Sigma_j(i\omega)\delta_{jj'}\delta_{mm'}, \tag{8}$$

and we need only find functions for the two spin-orbit states $j=5/2$ and $7/2$. This is an excellent approximation over most of the volume range studied here, including the volume-collapse regions, where the crystal-field splitting ranges from about 1 to 10% of the spin-orbit splitting. At the very smallest volumes considered here, this ratio approaches 50%; however, it is to be emphasized that this omission is only in the self-energy, and all such effects are reflected in $H^0_{\mathrm{LDA}}(\mathbf{k})$, where hybridization dominates anyway. In practice, we input a bath Green's function of similar structure, $\mathcal{G}_j\delta_{jj'}\delta_{mm'}$, into the QMC and then improve statistical uncertainties by averaging over the six $j=5/2$ and eight $7/2$ states in determining the output G^{imp}_j.

It was noted previously that the DMFT(QMC) iterations could be greatly accelerated by separately converging the leading, constant, Hartree-Fock-like part of the self-energy outside of the QMC part of the cycle.[36] For the present case, this constant part is

$$\Sigma^{(0)}_j = [n_f - n_j/(2j+1)]U_f. \tag{9}$$

Therefore, after each QMC cycle we extract just the frequency-dependent part of the self-energy,

$$\Delta\Sigma_j(i\omega) = \Sigma^{\mathrm{QMC}}_j(i\omega) - \Sigma^{(0)}_j(\{n^{\mathrm{QMC}}_j\}), \tag{10}$$

using here the QMC n_j values,

$$n^{\mathrm{QMC}}_j = (2j+1)[1 + \tilde{G}^{\mathrm{imp}}_j(0^+)], \tag{11}$$

where $\tilde{G}^{\mathrm{imp}}_j(\tau)$ is the imaginary time Fourier transform of $G^{\mathrm{imp}}_j(i\omega)$. Then with $\Delta\Sigma_j(i\omega)$ held fixed, we construct a new self-energy $\Sigma_j(i\omega)=\Sigma^{(0)}_j(\{n_j\})+\Delta\Sigma_j(i\omega)$, *but this time* taking the n_j defining $\Sigma^{(0)}$ as obtained from the lattice Green's function via Eq. (4). Inserting this self-energy back into the lattice Green's function Eq. (2) leads to a self-consistent condition on both $G_{\mathbf{k}}(i\omega)$ and the n_j, which may be completely converged with negligible cost, again with the $\Delta\Sigma_j$ held fixed. Only after this convergence would we take the resultant $G_{\mathbf{k}}(i\omega)$ and begin the process of mapping back onto the auxiliary impurity problem in order to update $\Delta\Sigma_j(i\omega)$.

We found the procedure of converging $\Sigma^{(0)}_j$ in between each QMC iteration for $\Delta\Sigma(i\omega)$ to work best when the current QMC ratio $n_{5/2}:n_{7/2}$ was retained during the cheap iterations, which were then used only to fix the total f charge n_f. Also note this approach requires the strict equivalence of the n_j calculation in both the lattice and impurity problems, which dictates using

$$G^{\mathrm{imp}}_{jm,j'm'}(i\omega) \equiv \frac{\delta_{jj'}\delta_{mm'}}{(2j+1)N}\sum_{\mathbf{k}} \mathrm{Tr}_{fj}\{G_{\mathbf{k}}(i\omega)\}, \tag{12}$$

in conjunction with Eq. (8) in solving Eq. (3) for the bath Green's function $\mathcal{G}_j\delta_{jj'}\delta_{mm'}$.

The output of each QMC cycle is the imaginary time Green's function $\tilde{G}^{\mathrm{imp}}_j(\tau)$, which contains statistical uncertainties and must be Fourier transformed in order to define the new self-energy $\Sigma_j(i\omega)$. Following earlier work,[35,36] our approach is to use multipole fits

$$\tilde{G}^{\mathrm{imp}}_j(\tau) \sim \tilde{F}_j(\tau) \equiv \sum_i w_{ji}\tilde{f}_i(\tau), \tag{13}$$

using basis functions $\tilde{f}_i(\tau) = -e^{-\varepsilon_i\tau}/(e^{-\beta\varepsilon_i}+1)$, which have Fourier transforms $f_i(i\omega)=1/(i\omega-\varepsilon_i)$, thus trivially giving the overall Fourier transforms. These fits were carried out requiring positive weights $w_{ji}\geqslant 0$ and constrained to give the QMC values at $\tau=0^+$,

$$\tilde{F}_j(0^+) = \tilde{G}^{\mathrm{imp}}_j(0^+) \tag{14}$$

as well as a number of correct moments $m=1,2,\ldots$

$$\tilde{F}^{(m-1)}_j(0^+) + \tilde{F}^{(m-1)}_j(\beta^-) = (-1)^m G^{(m)}_j. \tag{15}$$

Here $\beta^- = \beta - 0^+$, $\tilde{F}^{(m)}(\tau) \equiv (d^m/d\tau^m)\tilde{F}(\tau)$, and the high-frequency moments $G^{(m)}_j$ are defined by $G^{\mathrm{imp}}_j(i\omega) = \Sigma_m G^{(m)}_j/(i\omega)^m$. In our previous work on Ce, we imposed two $(m=1,2)$ of the constraints in Eq. (15); however, we find in the present effort for Pr and Nd at the largest volumes that it was necessary to add a third moment $(m=3)$. The reason is that for such strongly localized functions where the $\tilde{G}^{\mathrm{imp}}_j(\tau)$ fall rapidly away from their $\tau=0^+$ and β^- values, one may get large and unphysical values of $G^{(3)}_j$ and $G^{(4)}_j$ of opposite signs. This can lead to an unphysical structure in the spectra far from the chemical potential; although, we could detect no impact on the total energy or n_j from this problem. We found that adding the $m=3$ or $G^{(3)}_j$ constraint was sufficient to fix this difficulty.

The moments $G^{(m)}_j$ may be obtained from $\mathbf{k}$ averages and appropriate traces of powers of $H^0_{\mathrm{LDA}}(\mathbf{k})$ with additionally $\Sigma^{(0)}_j$ from Eq. (9) for $G^{(2)}_j$ and both $\Sigma^{(0)}_j$ and $\Sigma^{(1)}_j$ for $G^{(3)}_j$. $\Sigma^{(1)}_j$ may be obtained from the double occupation matrix[53] or approximated using a Hubbard-I type of self-energy tuned to give the QMC n_j values.

The results reported in this paper are for a temperature of 632 K(0.004 Ry), which given the T^{-3} cost of the QMC calculations is about as low as is practicable. Here the imaginary time interval $(0,\beta)$ for the QMC was discretized by $L=80$, 112, and 160 divisions, carrying out 10 000, 6000, and 2000 QMC sweeps, respectively, for each DMFT(QMC) iteration. The smaller number of sweeps for larger L was dictated purely by the L^3 expense of the calculations, and the statistical uncertainties necessarily increased. Nonetheless, systematic and generally L^{-2} behavior was seen allowing extrapolation to eliminate the Trotter errors.[54] Starting self-energies were already quite good and were taken from converged DMFT calculations with the Hubbard-I self-energy[36] or from nearby volumes or temperatures (0.01 Ry). At least 30 iterations were performed at each volume, following five discarded warm-up iterations. At a number of volumes, this process was repeated taking the final self-energy as the initial guess and starting the process from the beginning. The results were unchanged to well within the statistical uncertainties. All Matsubara sums for an argument $F(i\omega_n)e^{i\omega_n 0^+}$ were

carried out using an asymptotic two-pole approximation $F_{2pol}(i\omega)=w_1/(i\omega-\varepsilon_1)+w_2/(i\omega-\varepsilon_2)$ with the parameters fixed by the first four high-frequency moments of $F(i\omega)$. The infinite sum was then given by a finite sum over the difference $F(i\omega_n)-F_{2pol}(i\omega_n)$ plus the analytic result for the infinite sum over F_{2pol} with 256 positive Matsubara frequencies used in the former.

We found a noticeable increase in the QMC statistical uncertainties for the total energy in going from Ce to Pr to Nd, likely reflecting the larger role played by the potential energy U_fd and the QMC-determined value of the double occupation, Eq. (6), with the increasing number of $4f$ electrons. At large volumes, for example, d should be approximately 0, 1, and 3 for Ce, Pr, and Nd, respectively, at low temperatures. Similarly, we found differences in the nature of the Trotter corrections, where, again at larger volumes, we found the coefficient of the L^{-2} dependence to be quite small for Ce, larger for Pr, and significantly larger for Nd.

We were able to get decent spectra from the multipole fits Eq. (13) by increasing the number of poles by well over two orders of magnitude. As described earlier,[36] we took equally spaced ε_i grids of $L/4$ points and systematically eliminated poles with negative weights, examining $O(10^4)$ such grids of varying centroid and width to find the best fit. For the spectra, we combined the 30 best fits so long as the worst of these had a root-mean-square agreement with the QMC data no more than 20% larger than that of the best. More important, we also averaged over the fits for the last half of the DMFT(QMC) iterations. The resultant collections of $O(10^3)$ poles were broadened by Gaussians of 0.5 eV full width at half maximum. We found systematic evolution of these spectra with volume providing one measure of their validity.

C. Double occupation and moment

Since we approximate the f-f self-energy by the form $\Sigma_{jm,j'm'}(i\omega)=\Sigma_j(i\omega)\delta_{jj'}\delta_{mm'}$, a comparable treatment of the double occupation matrix is

$$\langle \hat{n}_{jm}\hat{n}_{j'm'}\rangle = \begin{cases} n_j/(2j+1) & \text{if } j=j', m=m' \\ d_{jj}/[j(2j+1)] & \text{if } j=j', m\neq m' \\ d_{5/2,7/2}/48 & \text{if } j\neq j' \end{cases}, \quad (16)$$

noting that $\hat{n}_{jm}^2=\hat{n}_{jm}$, and $j=5/2$ and $7/2$. We obtain n_j and $d_{jj'}$ from the QMC auxiliary impurity problem by summing over the appropriate blocks in the 14×14 matrix $\langle \hat{n}_{jm}\hat{n}_{j'm'}\rangle$. As these are block totals, the total number of f electrons per site is $n_f=n_{5/2}+n_{7/2}$, and the double occupation d appearing in the expression for the total energy is $d=d_{5/2,5/2}+d_{5/2,7/2}+d_{7/2,7/2}$. We find the present d_{jj} for $j=j'$ to be bounded above by their uncorrelated values from $\langle \hat{n}_{jm}\hat{n}_{jm'}\rangle \sim \langle \hat{n}_{jm}\rangle \times \langle \hat{n}_{jm'}\rangle$ for $m\neq m'$, or

$$d_j^{\text{unc}} = jn_j^2/(2j+1). \quad (17)$$

Similarly, we find the d_{jj} to be bounded below by a typical strongly correlated expression

$$d_{jj}^{\text{cor}} = l_j[n_j-(l_j+1)/2], \quad (18)$$

where l_j is an integer such that $l_j\leqslant n_j\leqslant l_j+1$ and Eq. (18) is a piecewise linear function of n_j with values $n_j(n_j-1)/2$ at integer n_j.

The expectation of the on-site squared f moment is given by $\langle \hat{J}^2\rangle=3\langle J_z^2\rangle$ since our Hamiltonian is rotationally invariant, and thence using Eq. (16) by

$$\langle \hat{J}^2\rangle = \sum_{j=5/2,7/2}(j+1)(jn_j-d_{jj}). \quad (19)$$

In the local-moment regime at large volume and low temperature where $n_{5/2}=1$, 2 and 3 for Ce, Pr, and Nd, respectively, $n_{7/2}=0$, and $d_{jj}=n_j(n_j-1)/2$, Eq. (19) yields $J=5/2$, 3.2749, and $7/2$, respectively, via $\langle \hat{J}^2\rangle=J(J+1)$. This compares to the Hund's rules ground state values of $J_{\text{true}}=5/2$, 4, and $9/2$, respectively, and reflects the fact that including the spin-orbit interaction in the absence of intra-atomic exchange will give the correct moment only when the $j=5/2$ subshell has a single electron or hole or is trivially empty or full. From the thermodynamic perspective, it is the degeneracy of the Hund's rules multiplet that matters, and this changes from $14!/[n!(14-n)!]=14$, 91, and 364 to $6!/[n!(6-n)!]=6$, 15, and 20 for Ce, Pr, and Nd, respectively, on adding spin orbit, which is quite an improvement given the correct degeneracy $2J_{\text{true}}+1=6$, 9, and 10, respectively. Although not described here, we do find DMFT calculations with the Hubbard-I self-energy to yield the expected low-temperature entropy plateaus of $\ln 6$, $\ln 15$, and $\ln 20$ in units of k_B for Ce, Pr, and Nd, respectively, at large volume, similar to earlier work for Ce without the spin-orbit interaction.[35,36]

One may use Eqs. (17) and (18) to find lower and upper bounds on $\langle \hat{J}^2\rangle$ in Eq. (19). If one assumes that the spin orbit is also quenched, $n_j=(2j+1)n_f/14$, in addition to the uncorrelated Eq. (17), then

$$\langle \hat{J}^2\rangle_{\text{unc}} = 51n_f(1-n_f/14)/4. \quad (20)$$

With this additional assumption, Eq. (20) no longer provides a lower bound on $\langle \hat{J}^2\rangle$ except at the smallest volumes where the spin orbit is quenched, but will nevertheless prove useful.

III. RESULTS

This section reports calculations for compressed Ce, Pr, and Nd obtained by the LDA+DMFT method with a QMC determination of the self-energy to be referred to more simply as just DMFT. All theoretical results have been carried out for an assumed fcc structure and at a temperature of 632 K(0.004 Ry) unless otherwise noted. This temperature is about as low as is practical given the T^{-3} expense of the QMC. Nevertheless, it appears cold enough since estimates for Ce of the change in the number of $4f$ electrons, the onsite $4f$ moment, and the total energy on halving the temperature to 316 K are all relatively small.[55] It should be emphasized that a model of the Ce phase diagram ascribes its predominant temperature dependence to the explicit T in the TS term of the free energy $F=E-TS$, and not from T dependence in either the energy or entropy.[56]

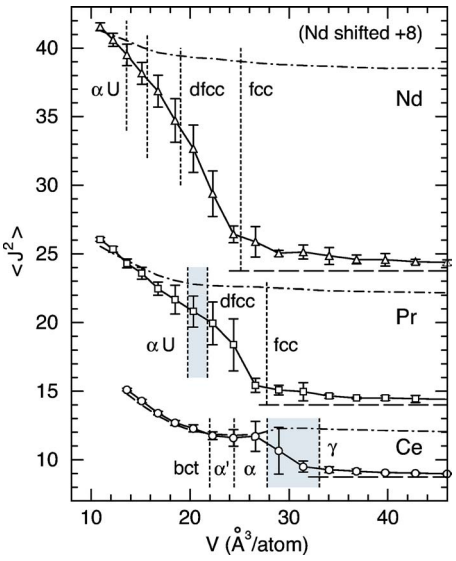

FIG. 1. (Color online) Squared local $4f$ moment $\langle J^2 \rangle$ for Ce, Pr, and Nd. The DMFT(QMC) results are given by the solid curves with data points; local-moment values, by the horizontal long-dashed lines; and an uncorrelated estimate with quenched spin orbit, by dash-dotted lines. The vertical short-dashed lines denote transitions, with significant volume collapse by shading. Both α and γ Ce phases are fcc.

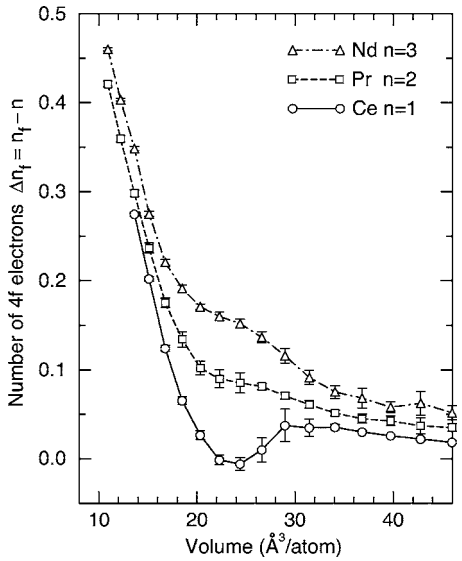

FIG. 2. Number of $4f$ electrons n_f less an integer $n=1$, 2, and 3 for Ce, Pr, and Nd, respectively.

A. Moment and spectra

The extended aspect of the evolution from localized to itinerant character in the three lanthanides is illustrated by the DMFT results (data points with error bars) in Fig. 1 for the square of the on-site $4f$ electron moment $\langle J^2 \rangle$ calculated using Eq. (19). The vertical dashed lines mark volumes at which transitions are observed experimentally. The horizontal long-dashed lines at large volume give the strongly correlated local-moment values $J(J+1)$ with J being the proper Hund's rules $5/2$ value for Ce, although somewhat smaller than the proper values for Pr and Nd due to our omission of intra-atomic exchange (see Sec. II C). It is apparent for each material that the local-moment regime persists under compression up to and through most of the stability field of the fcc phase (large volume γ fcc phase for Ce). The dash-dotted curves are uncorrelated approximations to $\langle J^2 \rangle$ from Eq. (20) which also presume that the spin orbit is quenched, i.e., that $n_{5/2}/n_{7/2} \sim 6/8$, which is largely responsible for the significant offset of these curves from the local-moment lines at large volume. The DMFT results approach these uncorrelated and spin-orbit quenched curves under compression, reaching reasonably close agreement by the α phase of Ce and α-U phases of Pr and Nd. As will be discussed subsequently, the significance of the quenched spin-orbit lies in the fact that the lower Hubbard band is of predominant $j=5/2$ character, while the $4f$ Kondo resonance, which grows at the Fermi level at the expense of the Hubbard side bands, is of mixed $j=5/2$, $7/2$ character. Therefore, quenched spin orbit reflects dominance of the Kondo peak, which may be viewed as a signature of itineracy.

A quantitative measure of the degree of correlation is provided by the lower (strongly correlated) and upper (uncorrelated) bounds on the double occupation given by Eqs. (17) and (18), respectively, which in turn provide bounds on $\langle J^2 \rangle$. The resultant curves have roughly the same shape as the DMFT results in Fig. 1 and bracket these results, in each case, with the DMFT curves switching from more or less perfect agreement with the strongly correlated limit at large volume to much closer to the uncorrelated limit at small volume. Even so, we find in the vicinity of $V \sim 12$ Å^3/atom that for each of these materials the DMFT results have switched only about 60% of the way from the strongly correlated to the totally uncorrelated limit, which is consistent with the fact that we still find residual Hubbard side bands at this volume. On the other hand, standard paramagnetic LDA certainly does well enough in predicting the c/a ratio in body-centered tetragonal (bct) Ce and structural characteristics of bct and α-U phases among the early actinides,[57,58] so it may well be that for all practical purposes such phases are weakly correlated enough.

The moment $\langle J^2 \rangle$ in Fig. 1 is a bare quantity and does not reflect any screening effects by the other electrons. Its large values at the smaller volumes are due via Eq. (19) to an increase in the number of $4f$ electrons n_f under compression as seen in Fig. 2, where $n_f - n$ is plotted with $n=1$, 2, and 3 for Ce, Pr, and Nd, respectively. It is well known that the lanthanides undergo electronic s-d transition under pressure, during which the $6s$ and $6p$ states begin to pass above the Fermi level, thereby, increasing the $5d$ and $4f$ occupations.[13] Figure 3 shows the fraction $n_{5/2}/n_f$ of $4f$ electrons which are of $j=5/2$ character, and it is quite clear that there is quenching of the spin orbit in the region of interest in this work.

The interplay between spin-orbit and compression-induced changes in $4f$ spectra may be seen in Fig. 4, where the total (Brillouin zone summed) but j-resolved $4f$ spectra or density of states $D_j(\varepsilon)$ is plotted for Pr at a number of volumes. These DMFT results were obtained by multipole fits to the QMC $\tilde{G}_j(\tau)$, as described in Sec. II B, and were broadened by a Gaussian of 0.5 eV full width at half maxi-

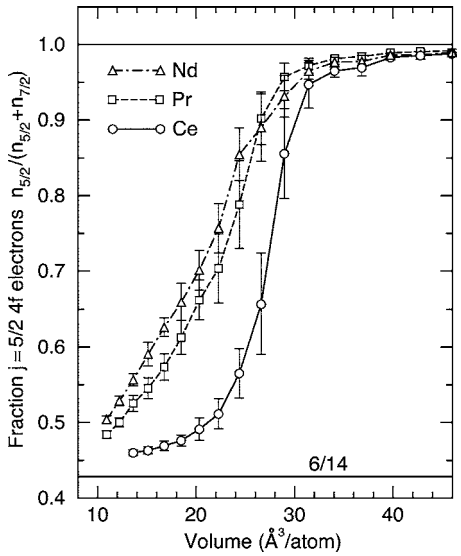

FIG. 3. Fraction of $4f$ electrons of $j=5/2$ character as a function of volume.

mum. At the largest volume $V=46.0$ Å^3/atom, one sees the pure $j=5/2$ lower Hubbard band near −5 eV and the mixed-j upper Hubbard band near 2 eV, with the splitting consistent with $U_f=6.4$ eV at this volume.[59] Under compression both Hubbard bands lose spectral weight at the expense of the growing Kondo peak near the chemical potential μ, which becomes dominant at the smallest volumes. Since this Fermi-level structure is also of mixed-j character, the population of these states at the expense of the initially pure $j=5/2$ lower Hubbard band relates the quenching of spin orbit in these materials to their growing itinerant character under compression. Note, however, as is especially evident at

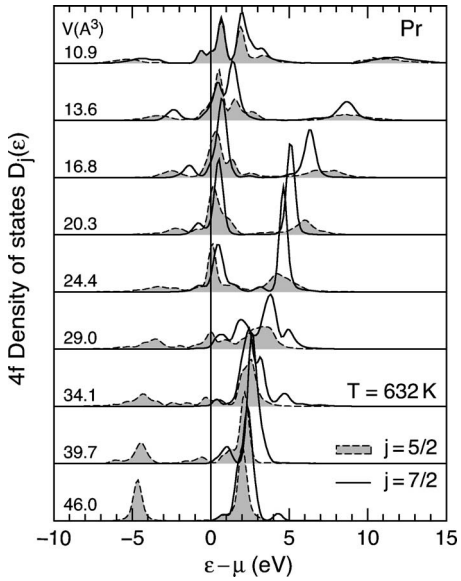

FIG. 4. Pr $4f$ density of states $D_j(\varepsilon)$ for $j=5/2$ (dashed line, shaded) and $j=7/2$ (solid line) as obtained from multipole fits to the QMC $\tilde{G}_j(\tau)$ with 0.5 eV FWHM Gaussian broadening. Areas are normalized 6:8 for the appropriate j's, and energy is relative to the chemical potential μ.

$V=24.4$ Å^3/atom, that the $j=5/2$ and $7/2$ contributions to the Kondo peak are split by about the spin-orbit energy,[60] with the former more centered at μ. Consequently, the occupied part of the Kondo peak is initially mostly $j=5/2$ character, although the $j=7/2$ part catches up as is also evident from Fig. 3. The Ce and Nd spectra are quite similar with the primary visual difference being the increasingly more prominent lower Hubbard band in the progression from Ce to Pr and Nd as is to be expected. The Ce spectra are available elsewhere.[35,36]

A cross check on the spectra in Fig. 4 is provided by

$$D_j(\mu) \sim (\beta/\pi)\tilde{G}_j(\beta/2), \tag{21}$$

where this expression becomes exact in the low-temperature limit.[61] Equation (21) tracks the values at $\varepsilon=\mu$ in Fig. 4 to within better than 20% at all volumes. The volume dependence of $D_{5/2}(\mu)$ from Eq. (21) looks very much like that plotted for Ce in the case without spin orbit in Fig. 3 of Ref. 35. For decreasing volume, these values are first quite small then rise to a maximum signifying growth of the Kondo peak and then begin to decrease as the hybridization-induced broadening of the $4f$ bands begins to dominate. Ce, Pr, and Nd all behave similarly with the onset of growth in the Kondo peak starting near the low-volume side of the fcc (γ-Ce) phases and then rising to successively higher maxima occurring at smaller volumes, roughly at 29, 23, and 20 Å^3/atom, respectively. Comparing these volumes with the transitions indicated in Fig. 1, it may be seen that the Ce value reaffirms earlier observations that the initial rapid rise of the Kondo peak in that material coincides with the volume collapse.[26–28,35,36] For Pr and Nd, on the other hand, the growth of the Kondo peak coincides with the observed stability field of the dfcc phase, suggesting a transitional role for this phase rather than being the end member of the localized trivalent lanthanide series as has been assumed. In contrast to the $j=5/2$ function, $D_{7/2}(\mu)$ starts to increase for decreasing volume at about the same place as $D_{5/2}(\mu)$, but does so more gradually, steadily growing until it becomes comparable to $D_{5/2}(\mu)$ at the smaller volumes.

B. Correlation energy

Figure 5(a) shows the Pr correlation energy, namely the total energy less the result $E_{\mathrm{HF}}(n_{\mathrm{loc}}=0)$ for a paramagnetic Hartree Fock solution of the effective Hamiltonian Eq. (1). One may obtain a variety of metastable Hartree Fock (HF) solutions in which different numbers n_{loc} of "localized" $4f$ bands are split off below the Fermi level, ranging from the paramagnetic solution $n_{\mathrm{loc}}=0$ to the fully spin-polarized and orbitally polarized solution (maximum n_{loc}), which in the case of $4f^2$ Pr is $n_{\mathrm{loc}}=2$. The γ phase of $4f^1$ Ce has been described by analogous fully polarized LDA+U solutions ($n_{\mathrm{loc}}=1$)[23,24] and the γ-α volume collapse by the $n_{\mathrm{loc}}=1\rightarrow 0$ transition.[23] Figure 5(a) suggests a two-step process in these HF solutions for Pr as first one split-off band pops back up to the Fermi level under compression (the $n_{\mathrm{loc}}=2$ and 1 curves cross) and then later the second does the same (the $n_{\mathrm{loc}}=1$ and 0 curves cross), a $n_{\mathrm{loc}}=2\rightarrow 1\rightarrow 0$ scenario for which there is no experimental evidence.

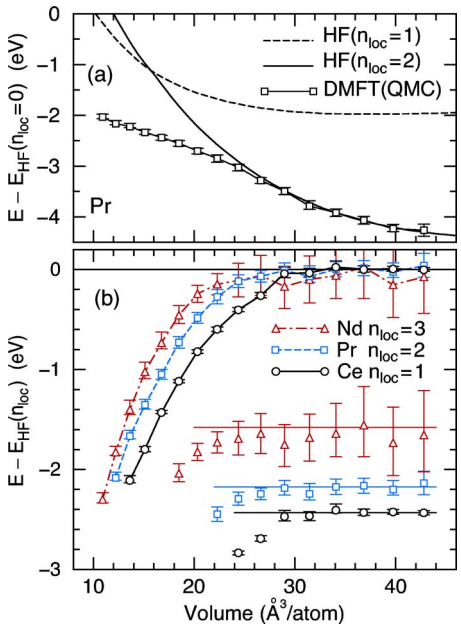

FIG. 5. (Color online) (a) Correlation energy for Pr as a function of volume. (b) The more interesting part of the Ce, Pr, and Nd correlation energies, namely the DMFT energies in each case less fully polarized Hartree Fock (HF). The insets (offset vertical axes) show the large volume behavior more clearly. The n_{loc} in $E_{\mathrm{HF}}(n_{\mathrm{loc}})$ refers to the number of $4f$ bands split off below the Fermi level in the HF calculations, with $n_{\mathrm{loc}}=0$ the customary paramagnetic solution, $n_{\mathrm{loc}}>0$ indicating spin-polarized and orbitally polarized solutions, and $n_{\mathrm{loc}}=1$, 2, and 3 for Ce, Pr, and Nd, respectively, being the fully polarized solutions.

On the other hand, there is some truth here, as the intermediate $n_{\mathrm{loc}}=1$ solution is really just a crude attempt to add $4f$ spectral weight at the Fermi level in the continued presence of some Hubbard splitting. For a truly correlated calculation, in contrast, there is an entirely continuous transfer of spectral weight from the Hubbard sidebands to the Kondo resonance at the Fermi level, consistent with the smooth behavior seen in the DMFT curve in Fig. 5(a). It agrees with the fully polarized HF result at large volumes (where the HF correctly captures the Hubbard splitting), but then bends smoothly away from this HF solution under compression (where the HF fails to describe the Kondo resonance). The same behavior has been seen in earlier DMFT results for Ce,[35,36] as well as in more rigorous QMC solutions for the Anderson lattice Hamiltonian.[62,63] It seems intuitively clear that such deviation from the fully polarized HF solution as volume is reduced should be associated with the growth of $4f$ spectral weight at the Fermi level, i.e., the Kondo resonance.

The total energy differences between DMFT and fully polarized HF solutions of Eq. (1) are shown in Fig. 5(b) for fcc Ce, Pr, and Nd. Ferromagnetic order was assumed for the HF. The three insets (shifted vertical axes) give a clearer view of the large volume behavior, and the systematically larger QMC uncertainties from Ce to Pr to Nd have been discussed in Sec. II B. Our calculations of the $4f$ spectra indicate growth of the Kondo resonance for each material first begins on the small-volume side of the experimentally observed fcc or γ-Ce stability range (see Fig. 1), and then $D_{5/2}(\mu)$ reaches a maximum at $\sim$29, 23, and 20 $Å^3$/atom for Ce, Pr, and Nd, respectively. These volumes are close to where the curves in Fig. 5(b) begin to bend away from the fully polarized HF (0 baseline), consistent with the association of this energy with the Kondo resonance.

The fact that these deviations occur at successively smaller volumes from Ce to Pr to Nd is consistent with the ratio of the Coulomb interaction to band width U_f/W_f for the $4f$ states, which near equilibrium volume ($\sim$34 $Å^3$/atom) is 3.7, 4.4, and 4.9 for Ce, Pr, and Nd, respectively.[13] Thus, Pr and Nd are successively more localized than Ce at ambient conditions, and greater compression is needed to bring about similar changes in electron correlation. A region of negative bulk modulus is of course essential to obtain a first-order isostructural transition as in Ce. If, more generally, a region of low bulk modulus were to favor larger-volume changes in structural phase transitions, then the delayed response of the softening effects in Fig. 5(b) for Pr and Nd means competing against the ever more dominant positive bulk moduli of the remaining contributions to the total energy as they continue to grow with decreasing volume. This is at least intuitively consistent with a 15% volume collapse in Ce, 9% in Pr, and apparently none in Nd. It is difficult to quantify this point as the QMC uncertainties in Fig. 5(b) do not admit very reliable calculations of the curvature of these results.

There are also some important differences between the Ce and Pr volume-collapse transitions, beyond the fact that the former is isostructural and the latter involves a structural change. As already noted, the experimentally observed two-phase region (27.8–33.1 Å^3/atom) for the γ-α collapse in Ce coincides with the region of rapid growth in the Kondo resonance. It also overlaps a rather sharp breakaway of the DMFT curve from the HF result as seen near 29 Å^3/atom in Fig. 5(b), which is consistent with a large negative contribution to the bulk modulus. Here, as for earlier results on Ce without the spin orbit,[35,36] as well as analyses of the Anderson lattice Hamiltonian,[62,63] these features corroborate the Kondo-volume-collapse model of the Ce γ-α transition.[26–28] For Pr, on the other hand, the volume collapse appears to occur at pressures above the region of rapid growth of the Kondo resonance. The maximum in the Pr $j=5/2$ spectral weight at the Fermi level is near 23 Å^3/atom (see also Fig. 4), and the Pr curve in Fig. 5(b) begins to bend away from the fully polarized HF at slightly larger volume, both of which lie outside and to the large-volume side of the observed two-phase region for Pr (19.8–21.8 Å^3/atom). If the Ce collapse serves to initiate the evolution from localized to itinerant in this material, such evolution is already well underway by the Pr collapse, a point which is also quite evident from behavior of the local moment in Fig. 1. X-ray spectroscopies may prove valuable in further elucidating such differences.[64,65]

C. Equation of state

Comparison of the theoretical and experimental energies are given for Ce, Pr, and Nd in Figs. 6–8, respectively. The HF and DMFT total energies are all at 632 K and for an

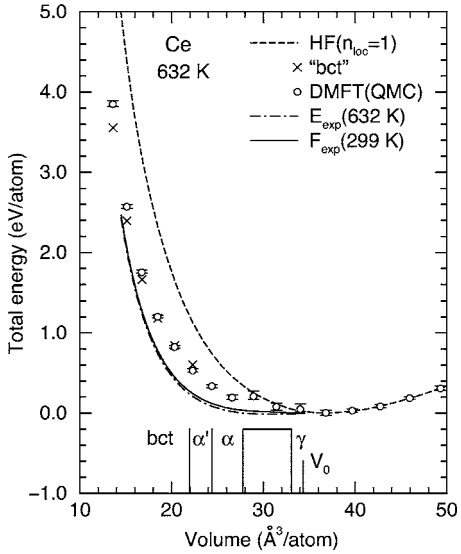

FIG. 6. Total energy of Ce as a function of volume. The theoretical HF and DMFT results are at 632 K. The experimental energy (632 K) and free energy (299 K) are obtained from Refs. 3 and 67 as described in the text. The theoretical bct estimate took a $T=0$ local-density bct-fcc energy difference (Ref. 66) and added this to the present fcc DMFT result. The experimentally observed 300-K equilibrium volume V_0 and stability fields for various phases are marked.

assumed fcc structure as noted. Experimental pressure data $P(V,T)$ exist for Pr over a wide range of volume at $300 \leqslant T \leqslant 725$ K and have been summarized by separate Birch-Murnaghan fits with temperature-dependent coefficients for

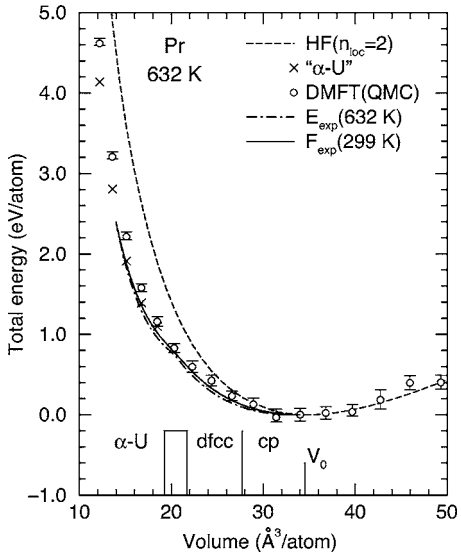

FIG. 7. Total energy of Pr as a function of volume. The theoretical HF and DMFT results are at 632 K. The experimental energy (632 K) and free energy (299 K) are obtained from Ref. 7 as described in the text. The theoretical α-U estimate took a $T=0$ local-density α-U–fcc energy difference (Ref. 19) and added this to the present fcc DMFT result. The experimentally observed 300-K equilibrium volume V_0 and stability fields for various phases are marked (cp denotes close packed).

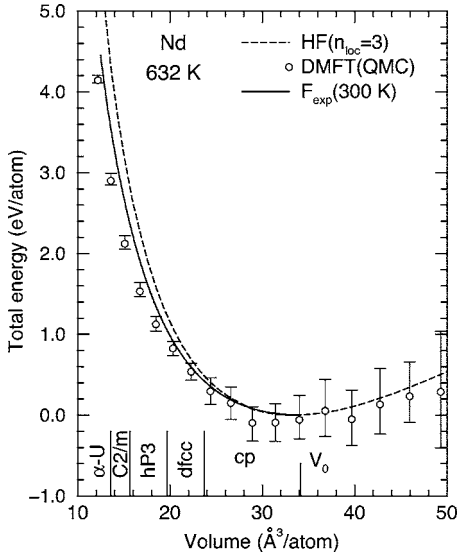

FIG. 8. Total energy of Nd as a function of volume. The theoretical HF and DMFT results are at 632 K. The experimental free energy (300 K) was obtained from Ref. 14. The experimentally observed 300-K equilibrium volume V_0 and stability fields for various phases are marked (cp denotes close packed).

the α-U phase lying at pressures above the collapse and the combined dfcc and fcc phases lying below, as well as by the linear dependence of the transition pressure on temperature.[7] These fits permit numerical evaluation of the free energy $F(V,T)=-\int dV P(V,T)$ and total energy $E(V,T)=-\int dV[P(V,T)-T\partial P(V,T)/\partial T]$ to the same accuracy as the pressure fits themselves, which appear in Fig. 4 of Ref. 7 to be quite reasonable. The constants of integration were fixed by setting $E(V_0,T)=F(V_0,T)=0$ at the experimental 300-K equilibrium volume V_0. Raising the temperature generally makes the free energy a steeper function of volume. However, since $\partial S/\partial V=\partial P/\partial T>0$, the total energy is generally less steep than the free energy. It is a fortunate coincidence that these effects roughly cancel so that the 300-K free energy is within 0.07 eV/atom of the 632-K total energy for Pr throughout the range plotted for these experimental quantities in Fig. 7, noting again that both are zeroed at V_0. Note that the volume dependence of the experimental entropy S is itself modest, in that TS increases by less than $\sim$0.2 eV/atom from $V=14$ to 35 Å^3/atom for both $T=300$ and 632 K.

Experimental measurements of $P(V,T)$ for Ce exist up to 208 GPa at 300 K[3] and over the temperature range 299–573 K within the fcc (α and γ) regime.[67] Integration of analytic fits to the room-temperature pressures immediately gives $F(V,300\text{ K})$ as above. Assuming $\partial P/\partial T$ is independent of volume within the bct and α' phases, one may use Ref. 3 to extend the higher-T isotherms of Ref. 67 to higher pressures. The resultant pressure-volume isotherms were then used to extrapolate two new isotherms at somewhat higher temperatures in the vicinity of 632 K, which provided the required $P(V,632\text{ K})$ and $\partial P(V,632\text{ K})/\partial T$ needed to obtain the 632-K total energy. While this procedure may introduce uncertainties, it is gratifying that the same $F(V,299\text{ K})\sim E(V,632\text{ K})$ result is seen in Fig. 6 for Ce as was found

TABLE I. Comparison of theoretical and experimental values for the equilibrium volumes V_0 (Å^3/atom) and bulk moduli B_0 (GPa). The theory used fits to the 632-K results in Figs. 6–8, while the experiment is at 300 K. However, the Ce HF results change by only 0.4% and −2.6% for V_0 and B_0, respectively, on reducing the temperature from 632 to 316 K.

	V_0^{HF}	V_0^{DMFT}	V_0^{expa}	B_0^{HF}	B_0^{DMFT}	B_0^{expb}
Ce	37.0	35.8	34.37	33.3	21.2	20–21
Pr	34.9	34.5	34.54	34.2	31.0	26–37
Nd	33.5	33.0	34.18	34.9	32.9	28–32

[a]From Ref. 69.
[b]From Ref. 70.

for Pr. We presume that it is also legitimate to compare room-temperature free energies for Nd to our 632-K calculated total energies for that material.

The Debye temperatures for Ce, Pr, and Nd are all below 150 K at ambient conditions,[68] and with reasonable Grüneisen parameters, all three materials should still be in the high-temperature limit at 632 K throughout the volume range studied here. The phonon contribution to the total energy is then $3k_BT$ and has no impact on the volume dependence examined in Figs. 6–8.

The total energies in Figs. 6–8 provide another perspective on the correlation issues discussed earlier. The fully polarized HF results (dashed) curves are analogous to LDA +U and should do well at large volumes in the strongly localized limit as is the case here. The DMFT results (open circles) then show how such static mean-field theories begin to break down as volume is reduced due to their inability to account for the growing Kondo resonance and its contribution to the correlation energy. This effect is most pronounced for Ce in Fig. 6, less so for Pr in Fig. 7, and smallest for Nd in Fig. 8, reflecting the fact that Pr and Nd start out successively further in the localized limit than Ce, therefore, requiring greater compression to achieve comparable changes in the correlation energy. Although the agreement between the DMFT results and the experimental isotherms is not ideal and will be discussed further, it is clear that the experiment does confirm this systematic progression.

A comparison of theoretical and experimental values for the bulk properties is given in Table I. The theory results were obtained from six-term fits[71] to the energies over the range 17–49 Å^3/atom in order to better average over the scatter in the QMC results. Table I shows quite decent agreement with experiment[72] and is a partial validation of the present effective Hamiltonians Eq. (1) and the manner of total-energy calculation Eq. (7). Of particular note is the fact that the DMFT results for V_0 and B_0 are in better agreement with the experiment and 3% and 36% smaller, respectively, than the fully polarized HF values in the case of Ce, as compared to ~1% and 6–9% smaller, respectively, for Pr and Nd. This suggests a small but not unimportant effect of the Kondo resonance even at $P=0$ in Ce, effects which are shifted to smaller volume and have less impact for Pr and Nd.

An estimate of the structural contribution to the energy at smaller volumes is provided by the "bct" and "α-U" results ($\times$ symbols) in Figs. 6 and 7 for Ce and Pr, respectively. These were obtained by adding paramagnetic local-density functional values for the bct-fcc energy difference in Ce[66] and the α-U–fcc difference in Pr[19] to the DMFT fcc values. Throughout the ranges shown in Figs. 6 and 7, these structural energy differences are 10% or less for Ce and 25% or less for Pr of the more dominant correlation energy contribution represented by the separation between the DMFT and the polarized HF curves. These structural corrections improve the agreement with the experiment somewhat for Ce and Pr; however, a similar correction for Nd would move the DMFT results to lower energies further away from the experiment.

Figure 9 gives the pressure-volume results corresponding to Figs. 6–8 with experimental 300-K data shown for Ce,[1–3] Pr,[4–8] and Nd.[14,73,74] Except for the $T=0$ LDA results (thin solid lines),[75] the theoretical results are negative volume derivatives of the 632-K total energies in these figures, an approximation justified by the $F_{\mathrm{exp}}(300\ \mathrm{K}) \sim E_{\mathrm{exp}}(632\ \mathrm{K})$ comparisons in Figs. 6 and 7. Multiterm fits to the energies were used in obtaining the derivatives.[71] The DMFT points (open circles) were fit ignoring the error bars, with separate fits made for the regions above and below the observed collapse transitions for Ce and Pr. It is evident that the present paramagnetic DMFT results do well in both low-pressure localized and high-pressure itinerant extremes, especially considering the structural corrections [dashed lines in Figs. 9(a) and 9(b)] in the later regime, although there are evident discrepancies in between as will be discussed. Standard paramagnetic LDA does well in the itinerant regime as seen by the thin black lines, but must be combined with one of the magnetically ordered modified-LDA techniques (e.g., LDA+U) to capture the larger volume behavior. This then leads to a magnetic order-disorder transition, which is not observed at room temperature, and, e.g., to an incorrect prediction of a volume collapse (16% at 39 GPa) in Nd.[18]

Turning to the collapse transitions, the kink in the DMFT total energy for Ce near 29 Å^3/atom in Fig. 6 lies within the experimental two-phase region, is within the QMC error bars, and is similar to earlier results without spin orbit.[35,36] It would appear to be a meaningful signature of the Ce transition. The addition of the spin-orbit interaction has lowered the γ-phase energy more than that of the α phase, so that a common tangent construction to the DMFT energy curve in Fig. 6 gives a pressure of 4 ± 2 GPa as compared to a slightly negative value in the earlier work. While the experimental transition ranges from (an extrapolated) −0.7 GPa at

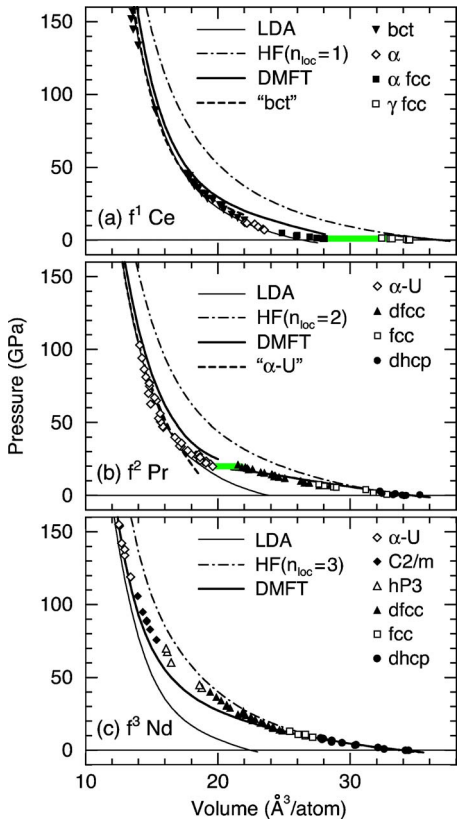

FIG. 9. (Color online) Experimental 300-K pressure-volume data for (a) Ce (Refs. 1–3), (b) Pr (Refs. 4–8), and (c) Nd (Refs. 14, 73, and 74) as compared to theory. The observed volume-collapse transitions in Ce and Pr are shaded. The thin solid lines give $T=0$ LDA results (Ref. 75), while the HF, DMFT, and structural estimates (bct Ce, α-U Pr) are negative volume derivatives of the total energies in Figs. 6–8.

$T=0$ to 1.8 GPa at 485 K,[67] an error of 4 GPa is not huge on the scale of Fig. 9(a). The volume change at 4 GPa in the DMFT results (thick solid lines) in Fig. 9(a) is in decent agreement with that observed at room temperature.

In the case of Pr, the experimental free energy (solid line) in Fig. 7 is linear over the two-phase region as it integrates a constant pressure, while the experimental total energy (dash-dotted curve) shows a slight negative curvature. Both curves reflect the dfcc to α-U structural change which takes place across the transition. While the contribution from Fig. 5(b) leads to a softening in the DMFT total energy for fcc Pr in Fig. 7 (open circles), there is no convincing evidence in the present work for a region of negative bulk modulus as might drive a fcc-to-fcc isostructural transition. It is possible that improvements such as inter-LDA-DMFT self-consistency might create such an isostructural transition;[49] however, it may also be that there should be no collapse in a pure fcc phase. Certainly, the estimated α-U structural corrections to the present fcc DMFT Pr results agree fairly well with the experiment for both total energy (Fig. 7) and pressure [Fig. 9(b)], and the present implementation does obtain a meaningful signature of the isostructural Ce transition.

Finally, we turn to the discrepancies between theory and experiment in Figs. 6–9. The fact that the DMFT results for Ce in Fig. 6 are too high at smaller volumes in comparison with experiment, those for Pr in Fig. 7 are reasonable, while those for Nd in Fig. 8 are somewhat low is suggestive of the intra-atomic exchange interaction K, which has been omitted in the present work. In the strongly localized regime including $V\sim V_0$, this exchange interaction should shift the energy by 0, $-K$, and $-3K$ for Ce, Pr, and Nd, respectively. At small volumes, the itinerant expectation would be $-K\Sigma_\sigma\Sigma_{m<m'}\langle n_{m\sigma}n_{m'\sigma}\rangle\sim -3Kn_f^2/14$ taking $\langle n_{m\sigma}n_{m'\sigma}\rangle \sim (n_f/14)^2$. If the total energies are shifted to 0 at V_0 as done in these figures, this would suggest shifts of −0.31, 0.08, and 0.69 eV at $V=15$ Å^3/atom for Ce, Pr, and Nd, respectively, taking values of n_f from Fig. 2 and $K\sim 1$ eV. This would imply completely itinerant states at 15 Å^3/atom, which is unlikely especially for Nd. Indeed, polarized HF calculations suggest exchange corrections at this volume of −0.13, 0.07, and 0.25 eV,[76] respectively, although this also is only an estimate. Nevertheless, these estimates do suggest that intra-atomic exchange would significantly improve the present comparisons between theory and experiment.

Unfortunately, a rigorous inclusion of the exchange interaction, one that would also yield the correct Hund's rules values for the Pr and Nd local moments, would require DMFT calculations for the full f-f Coulomb interaction including all four Slater integrals and the non-density-density exchange and pair hopping terms. This has been a challenge for QMC, although there is recent progress.[77] Similarly, implementing mutual self-consistency between the LDA and DMFT parts of the calculations, as has been advocated,[49] would be prohibitively expensive with the present QMC implementation of the self-energy. Both improvements as well as DMFT calculations of the structural energy differences could be considered with faster although less rigorous approaches to the self-energy,[78] which would appear to be the natural next step in trying to better understand the high-pressure behavior of the lanthanides.

IV. SUMMARY AND DISCUSSION

A better understanding of the electron-correlation-driven volume-collapse transitions in the compressed lanthanides may come from putting this behavior in context of their extended evolution from localized to itinerant character. To this end, the present paper has reported calculations for compressed Ce ($4f^1$), Pr ($4f^2$), and Nd ($4f^3$) using a combination of the local-density approximation (LDA) and dynamical mean-field theory (DMFT), the so-called LDA+DMFT. Results for the $4f$ moment $\langle\hat{J}^2\rangle$, spectra, correlation energy, and equation of state among other quantities have been presented over a wide range of volume at a temperature of 632 K. This temperature is the lowest feasible with the present quantum Monte Carlo (QMC) implementation of the self-energy, yet it appears reasonably close to the low-temperature limit for such quantities as n_f,$\langle\hat{J}^2\rangle$, and the total energy.[55] While a face-centered cubic (fcc) structure was assumed, LDA estimates of the important structural energy differences are significantly smaller than the relevant contributions to the correlation energy which may then be described as the leading order volume-dependent effects.

We find the three lanthanides to remain rather strongly localized under compression from ambient conditions up through the observed stability fields of the fcc (γ-Ce) phases, in the sense that the $4f$ moments are close to the Hund's rules values, there are fully formed Hubbard sidebands, which are themselves a signature of the local moments, and little $4f$ spectral weight lying in between at the Fermi level. Subsequent compression brings about a significant deviation of the moments from the Hund's rules values, growth of $4f$ spectral weight at the Fermi level (the Kondo resonance) at the expense of the Hubbard side bands, an associated softening in the total energy, and quenching of the spin orbit given that the Kondo peak is of mixed-j character in contrast to the predominantly $j=5/2$ lower Hubbard band. The most dramatic evolution in these signatures is seen to coincide with the two-phase region of the γ-α phase transition in the case of Ce, which is consistent with earlier work,[34–36] and in agreement with the Kondo-volume-collapse scenario.[26–28] For Pr and Nd, on the other hand, these signatures change most rapidly over the volume range where the distorted fcc (dfcc) structure is experimentally observed to be stable, suggesting that this phase is transitional and not part of the localized trivalent lanthanide sequence.

Only on subsequent compression is Pr experimentally observed to undergo a collapse from the dfcc phase to an α-U structure, while Nd passes from dfcc to α-U through two other low-symmetry phases without any substantial volume changes. Due to the increasing but incompletely screened nuclear charge, the lanthanides shift toward the localized limit for the larger atomic number, and we see a similar offset to smaller volume of the above-mentioned signatures from Ce to Pr and then Nd. In particular, a softening contribution to the total energy associated with growth of the Kondo resonance must compete with the remaining contributions which become ever more dominant due to a steadily increasing bulk modulus as volume is reduced. If a region of low bulk modulus were to favor larger-volume changes in structural transitions, then this would be qualitatively consistent with the observed sequence 15% (Ce), 9% (Pr), and none (Nd). This speculation is apparently contradicted by the 5% and 6% collapse transitions in Gd ($4f^7$) and Dy ($4f^9$), respectively. However, these lanthanides correspond to filling a different spin-orbit subshell, which may significantly complicate matters given the profound manner in which spin orbit is involved.

There are still some correlation effects evident at even the smallest volumes considered here, such as residual Hubbard side bands in the $4f$ spectra and moments whose values have evolved only $\sim$60% of the way from the strongly localized Hund's rules values to those characteristic of totally uncorrelated electrons. Nevertheless, standard paramagnetic LDA does quite well within the bct phase of Ce and the α-U phases of Pr and Nd, and so for all practical purposes, these phases appear weakly correlated enough. The success of LDA calculations for the structural parameters in these phases for Ce as well as the light actinides is also well known.[57,58]

This work has also included a detailed quantitative comparison between the present LDA+DMFT results and the experiment for the total energies and pressures of Ce, Pr, and Nd. The comparison is encouraging and serves to corroborate such theoretical observations as the systematic offset of Kondo-like correlation signatures to smaller volume for increasing atomic number in these three lanthanides. There are also clear deficiencies, most notably the need to include the intra-atomic exchange, ideally in its full rotationally invariant form to enable rigorous calculation of the Hund's rules moments in general cases. The need for accurate LDA+DMFT structural energy differences is also apparent. These improvements as well as making the LDA and DMFT parts mutually self-consistent will require a self-energy treatment that is both more precise and considerably less expensive, which unfortunately is likely to require giving up some of the rigor of the present QMC approach.

ACKNOWLEDGMENTS

This work was performed under the auspices of the U.S. Department of Energy by the University of California, Lawrence Livermore National Laboratory under Contract No. W-7405-Eng-48. The author gratefully acknowledges extended interactions with Stewardship Science Academic Alliances collaborators at U.C. Davis (DOE/NNSA Grant No. NA00071), especially R. T. Scalettar. He has benefited from conversations with K. Held and with members of the DOE/BES-funded Computational Materials Science Network Cooperative Research Team on "Predictive Capability for Strongly Correlated Systems." A modification of the QMC code of Ref. 30 (App. D) was used in the present work.

[1] D. G. Koskimaki and K. A. Gschneidner Jr., in *Handbook on the Physics and Chemistry of Rare Earths*, edited by K. A. Gschneidner Jr. and L. R. Eyring (North-Holland, Amsterdam, 1978), p. 337.

[2] J. S. Olsen, L. Gerward, U. Benedict, and J. P. Itié, Physica B & C **133B**, 129 (1985).

[3] Y. K. Vohra, S. L. Beaver, J. Akella, C. A. Ruddle, and S. T. Weir, J. Appl. Phys. **85**, 2451 (1999).

[4] H. K. Mao *et al.*, J. Appl. Phys. **52**, 4572 (1981); G. S. Smith and J. Akella, J. Appl. Phys. **53**, 9212 (1982); W. A. Grosshans and W. B. Holzapfel, J. Phys. (Paris) **45**, C8 (1984).

[5] Y. C. Zhao, F. Porsch, and W. B. Holzapfel, Phys. Rev. B **52**, 134 (1995).

[6] G. N. Chesnut and Y. K. Vohra, Phys. Rev. B **62**, 2965 (2000).

[7] B. J. Baer, H. Cynn, V. Iota, C-S. Yoo, and G. Shen, Phys. Rev. B **67**, 134115 (2003).

[8] N. C. Cunningham, N. Velisavljevic, and Y. K. Vohra, Phys. Rev. B **71**, 012108 (2005).

[9] H. Hua, Y. K. Vohra, J. Akella, S. T. Weir, R. Ahuja, and B. Johansson, Rev. High Pressure Sci. Technol. **7**, 233 (1998).

[10] R. Patterson, C. K. Saw, and J. Akella, J. Appl. Phys. **95**, 5443 (1004).
[11] U. Benedict, J. Alloys Compd. **193**, 88 (1993).
[12] W. B. Holzapfel, J. Alloys Compd. **223**, 170 (1995).
[13] A. K. McMahan, C. Huscroft, R. T. Scalettar, and E. L. Pollock, J. Comput.-Aided Mater. Des. **5**, 131 (1998).
[14] G. N. Chesnut and Y. K. Vohra, Phys. Rev. B **61**, R3768 (2000).
[15] S. Heathman, R. G. Haire, T. Le Bihan, A. Lindbaum, K. Litfin, Y. Méresse, and H. Libotte, Phys. Rev. Lett. **85**, 2961 (2000); A. Lindbaum, S. Heathman, K. Litfin, Y. Méresse, R. G. Haire, T. Le Bihan, and H. Libotte, Phys. Rev. B **63**, 214101 (2001).
[16] B. Johansson, Philos. Mag. **30**, 469 (1974).
[17] B. Johansson, Phys. Rev. B **11**, 2740 (1975).
[18] O. Eriksson, M. S. S. Brooks, and B. Johansson, Phys. Rev. B **41**, R7311 (1990).
[19] P. Söderlind, Phys. Rev. B **65**, 115105 (2002).
[20] A. Svane, J. Trygg, B. Johansson, and O. Eriksson, Phys. Rev. B **56**, 7143 (1997).
[21] A. Svane, Phys. Rev. Lett. **72**, 1248 (1994); Phys. Rev. B **53**, 4275 (1996).
[22] Z. Szotek, W. M. Temmerman, and H. Winter, Phys. Rev. Lett. **72**, 1244 (1994).
[23] I. S. Sandalov, O. Hjortstam, B. Johansson, and O. Eriksson, Phys. Rev. B **51**, 13987 (1995).
[24] A. B. Shick, W. E. Pickett, and A. I. Liechtenstein, J. Electron Spectrosc. Relat. Phenom. **114**, 753 (2001).
[25] K. Held, C. Huscroft, R. T. Scalettar, and A. K. McMahan, Phys. Rev. Lett. **85**, 373 (2000).
[26] J. W. Allen and R. M. Martin, Phys. Rev. Lett. **49**, 1106 (1982).
[27] M. Lavagna, C. Lacroix, and M. Cyrot, Phys. Lett. **90A**, 210 (1982).
[28] J. W. Allen and L. Z. Liu, Phys. Rev. B **46**, 5047 (1992).
[29] D. Vollhardt, in *Correlated Electron Systems*, edited by V. J. Emery (World Scientific, Singapore, 1993), p. 57; Th. Pruschke, M. Jarrell, and J. K. Freericks, Adv. Phys. **44**, 187 (1995).
[30] A. Georges, G. Kotliar, W. Krauth, and M. Rozenberg, Rev. Mod. Phys. **68**, 13 (1996).
[31] V. I. Anisimov, A. I. Poteryaev, M. A. Korotin, A. O. Anokhin, and G. Kotliar, J. Phys.: Condens. Matter **9**, 7359 (1997).
[32] A. I. Lichtenstein and M. I. Katsnelson, Phys. Rev. B **57**, 6884 (1998).
[33] For a tutorial, see K. Held, I. A. Nekrasov, G. Keller, V. Eyert, N. Blümer, A. K. McMahan, R. T. Scalettar, T. Pruschke, V. I. Anisimov, and D. Vollhardt, in *Quantum Simulations of Complex Many-Body Systems: From Theory to Algorithms*, edited by J. Grotendorst, D. Marx, and A. Muramatsu, NIC Series Vol. 10 (NIC Directors, Forschungszentrum Jülich, 2002), p. 175–209; cond-mat/0112079 (unpublished).
[34] M. B. Zölfl, I. A. Nekrasov, Th. Pruschke, V. I. Anisimov, and J. Keller, Phys. Rev. Lett. **87**, 276403 (2001).
[35] K. Held, A. K. McMahan, and R. T. Scalettar, Phys. Rev. Lett. **87**, 276404 (2001).
[36] A. K. McMahan, K. Held, and R. T. Scalettar, Phys. Rev. B **67**, 075108 (2003).
[37] K. Haule, V. Oudovenko, S. Y. Savrasov, and G. Kotliar, Phys. Rev. Lett. **94**, 036401 (2005).
[38] S. Y. Savrasov, G. Kotliar, and E. Abrahams, Nature (London) **410**, 793 (2001).
[39] N. Hamaya, Y. Sakamoto, H. Fujihisa, Y. Fujii, K. Takemura, T. Kikegawa, and O. Shimomura, J. Phys.: Condens. Matter **5**, L369 (1993).
[40] Y. K. Vohra, H. Olijnik, W. Grosshans, and W. B. Holzapfel, Phys. Rev. Lett. **47**, 1065 (1981).
[41] J. C. Duthie and D. G. Pettifor, Phys. Rev. Lett. **38**, 564 (1977).
[42] J. D. Thompson, Z. Fisk, J. M. Lawrence, J. L. Smith, and R. M. Martin, Phys. Rev. Lett. **50**, 1081 (1983).
[43] A rapid drop in entropy across the γ-α collapse in Ce may be viewed via $S(V,T)=\int_0^T dT' C_V(V,T')/T'$ as arising from a specific heat $C_V(V,T)$ peak, which lies below, e.g., $T=300$ K on the larger-volume γ side, but moves above 300 K on the smaller-volume α side. The finite-T total energy, $E(V,T)=E_0(V)+\int_0^T dT' C_V(V,T')$, should then show a concomitant softening near the collapse, possibly even a region of negative curvature, even though it is the free energy which dictates the transition, regardless of whether the $T=0$ energy $E_0(V)$ is featureless.
[44] J. E. Hirsch and R. M. Fye, Phys. Rev. Lett. **56**, 2521 (1986).
[45] See Ref. 30 and M. Jarrell, in *Numerical Methods for Lattice Quantum Many-Body Problems*, edited by D. Scalapino (Addison-Wesley, Reading, MA 1997) for one-band DMFT(QMC).
[46] O. K. Andersen, Phys. Rev. B **12**, 3060 (1975).
[47] H. L. Skriver, *The LMTO Method* (Springer, Berlin, 1984).
[48] Details of the present linear muffin-tin orbital (LMTO) calculations for lanthanides are given in A. K. McMahan, H. L. Skriver, and B. Johansson, Phys. Rev. B **23**, 5016 (1981).
[49] S. Y. Savrasov and G. Kotliar, Phys. Rev. B **69**, 245101 (2004).
[50] S. Biermann, F. Aryasetiawan, and A. Georges, Phys. Rev. Lett. **90**, 086402 (2003).
[51] P. Sun and G. Kotliar, Phys. Rev. Lett. **92**, 196402 (2004).
[52] In the full cubic point group, $\Sigma(i\omega)$ would be characterized by five unique diagonal matrix elements corresponding to the irreducible representations $\Gamma_6^-(j=7/2)$, $\Gamma_7^-(5/2 \text{ and } 7/2)$, Γ_8^- (5/2 and 7/2), with unique off-diagonal couplings between the two Γ_7^- and between the two Γ_8^-.
[53] V. Oudovenko, K. Haule, S. Y. Savrasof, D. Villani, and G. Kotliar, cond-mat/0401539 (unpublished); see Appendix A.
[54] R. M. Fye, Phys. Rev. B **33**, 6271 (1986).
[55] Halving the temperature from 632 to 316 K changes the total energy and n_f for Ce by less than 0.008 eV/atom and $\sim$0.1%, respectively, throughout the volume range examined in this paper, for both HF and DMFT with the Hubbard-I self-energy. Estimates of DMFT(QMC) total energies at 316 K based on just $L=112$ and 160 agree with the 632-K values to within $\pm$0.05 eV/atom over the 25–35 Å^3/atom volume range near the Ce transition. Similarly, DMFT(QMC) values of n_f and $\langle \hat{J}^2 \rangle$ at 632 and 316 K agree well inside their statistical uncertainties.
[56] B. Johansson, I. A. Abrikosov, M. Aldén, A. V. Ruban, and H. L. Skriver, Phys. Rev. Lett. **74**, 2335 (1995).
[57] M. S. S. Brooks, B. Johansson, and H. L. Skriver, in *Handbook on the Physics and Chemistry of the Actinides*, edited by A. J. Freeman and G. H. Lander (North-Holland, Amsterdam, 1984), Vol. 1, p. 153.
[58] P. Söderlind, Adv. Phys. **47**, 959 (1998).
[59] The Hubbard U_f values for Ce, Pr, and Nd are plotted in Ref. 13, and, e.g., for Pr are 6.4, 5.9, and 4.7 eV for $V=46.0$, 29.0, and 10.9 Å^3/atom, respectively.
[60] Spin-orbit splitting of the Kondo resonance has been previously seen in photoemission data for Ce: F. Patthey, B. Delley, W-D. Schneider, and Y. Baer, Phys. Rev. Lett. **55**, 1518 (1985).
[61] N. Trivedi and M. Randeria, Phys. Rev. Lett. **75**, 312 (1999).

[62] C. Huscroft, A. K. McMahan, and R. T. Scalettar, Phys. Rev. Lett. **82**, 2342 (1999).
[63] T. Paiva, G. Esirgen, R. T. Scalettar, C. Huscroft, and A. K. McMahan, Phys. Rev. B **68**, 195111 (2003).
[64] J. Röhler and R. Lübbers, [Physica B **206 & 207**, 368 (1995)] suggest that the L_{III} x-ray absorption line changes across the collapse transition in Ce, but not in Pr. More recent L_{III} measurements do see some change in the Pr case [C-S. Yoo (private communication)].
[65] J-P. Rueff, C. F. Hague, J-M. Mariot, L. Journel, R. Delaunay, J-P. Kappler, G. Schmerber, A. Derory, N. Jaouen, and G. Krill, Phys. Rev. Lett. **93**, 067402 (2004).
[66] P. Ravindran, L. Nordstrom, R. Ahuja, J. M. Wills, B. Johansson, and O. Eriksson, Phys. Rev. B **57**, 2091 (1998). See Fig. 10.
[67] A. Schiwek, F. Porsch, and W. B. Holzapfel, High Press. Res. **22**, 407 (2002).
[68] K. A. Gschneidner Jr., in *Solid State Physics*, edited by F. Seitz and D. Turnbull (Academic Press, London, 1965), Vol. 16, p. 275.
[69] K. A. Gschneidner Jr., Bull. Alloy Phase Diagrams **11**, 216 (1990).
[70] W. A. Grosshans and W. B. Holzapfel, Phys. Rev. B **45**, 5171 (1992).
[71] We fit the energies to expansions in powers of $V^{-2/3}$ following F. Birch, J. Geophys. Res. **57**, 227 (1952).
[72] A. Delin, L. Fast, B. Johansson, O. Eriksson, and J. M. Wills, Phys. Rev. B **58**, 4345 (1998).
[73] J. Akella, and G. S. Smith, J. Less-Common Met. **116**, 313 (1986); J. Akella, J. Xu, and G. S. Smith, Physica B & C **139 & 140B**, 285 (1986).
[74] J. Akella, S. T. Weir, Y. K. Vohra, H. Prokop, S. A. Catledge, and G. N. Chesntnut, J. Phys.: Condens. Matter **11**, 6515 (1999).
[75] These are LMTO atomic-sphere approximation calculations including the combined and Ewald corrections for a fcc structure.
[76] To test exchange, we performed fully polarized HF calculations with and without the Slater integrals F^k for $k \geqslant 2$, using $F^4/F^2 = 0.7018$, and $F^6/F^2 = 0.5366$ [G. H. Dieke, *Spectra and Energy Levels of Rare Earth Ions in Crystals*, edited by H. M. Crosswhite and H. Crosswhite (Interscience, New York, 1968), p. 63]. We identified the monopole integral F^0 with the LDA constrained occupation result U_f, approximated Dieke's result for F^2 by $(1.369+0.019n_f)U_f$ for integer n_f, and used the volume-dependent U_f to scale all parameters.
[77] S. Sakai, R. Arita, and H. Aoki, Phys. Rev. B **70**, 172504 (2004).
[78] S. Y. Savrasov, V. Oudovenko, K. Haule, D. Villani, and G. Kotliar, Phys. Rev. B **71**, 115117 (2005).